High order integral equation method for diffraction gratings

Wangtao Lu[1,2,3] and Ya Yan Lu[3]

[1] *Joint Advanced Research Center of University of Science and Technology of China and City University of Hong Kong, Suzhou, Jiangsu, China*

[2] *School of Mathematical Sciences, University of Science and Technology of China, Hefei, Anhui, China*

[3] *Department of Mathematics, City University of Hong Kong, Kowloon, Hong Kong*

Conventional integral equation methods for diffraction gratings require lattice sum techniques to evaluate quasi-periodic Green's functions. The boundary integral equation Neumann-to-Dirichlet map (BIE-NtD) method (Wu *et al.*, J. Opt. Soc. Am. A **26**, 2444-2451, 2009; **28**, 1191-1196, 2011) is a recently developed integral equation method that avoids the quasi-periodic Green's functions and is relatively easy to implement. In this paper, we present a number of improvements for this method, including a revised formulation that is more stable numerically, and more accurate methods for computing tangential derivatives along material interfaces and for matching boundary conditions with the homogeneous top and bottom regions. Numerical examples indicate that the improved BIE-DtN map method achieves high order of accuracy for in-plane and conical diffractions of dielectric gratings. © 2012 Optical Society of America

OCIS codes: 050.1755,050.1960,000.4430.

1. Introduction

Diffraction gratings and other periodic structures are important optical components that can be used to control and manipulate light [1,2]. Efficient numerical methods are needed to analyze the diffraction and scattering of light by these periodic structures. Existing numerical methods for diffraction gratings include general-purpose methods such as the finite-difference time-domain (FDTD) method and the finite element method (FEM) [3], and more special methods such as the analytic modal method [4–7], numerical modal methods [8–18], the

boundary integral equation (BIE) methods [19–28], etc. Although FDTD and FEM are extremely versatile, they are typically less efficient than the special methods. Numerical modal methods, especially the Fourier modal method (FMM) [8–12], are simple to implement and very popular, but they also have a number of limitations [11,29]. Conventional BIE methods are applicable to gratings with piecewise constant but otherwise arbitrary refractive index profiles, but they are relatively complicated to implement since the quasi-periodic Green's function appeared in the integral operators require sophisticated lattice sum techniques to evaluate. For gratings with high index-contrast and sharp corners in their profiles, all analytic and numerical modal methods converge slowly and may even fail to converge, due to the possible field singularity at the corners. The BIE methods may be able to treat the corner singularity more accurately. A version developed by Goray and Schmidt [27] based on a boundary element discretization appears to have a third order of accuracy even when the grating profiles have corners.

The boundary integral equation Neumann-to-Dirichlet map (BIE-NtD) method [30, 31] is a recently developed variant of the BIE methods that avoids the quasi-periodic Green's function, and it is relatively easy to implement. The method divides one period of a grating into a few subdomains of constant refractive index, constructs a relation (the so-called NtD map) on the boundary of each subdomain between $\partial_{\boldsymbol{\nu}} u$ and u where u is any component of the electromagnetic field and $\partial_{\boldsymbol{\nu}} u$ is its normal derivative, and solves the diffraction problem based on the NtD maps. A BIE is used to find the NtD map for each homogeneous subdomain, and the involved integral operators are related to the standard Green's function of the Helmholtz equation. Numerical examples given in Refs. [30, 31] indicate that the BIE-NtD method gives accurate solutions even when the grating profiles have sharp corners. However, the order of accuracy is not clear and the method appears to be less accurate for conical diffraction problems. In this paper, we present an improved version of the BIE-NtD method for both in-plane and conical diffraction problems. We calculate a modified NtD map, develop accurate approximations for the boundary conditions terminating the top and bottom homogeneous media, and use a new technique to approximate tangential derivatives on material interfaces. Several numerical examples are presented to demonstrate the high order of accuracy of our improved BIE-NtD method for dielectric gratings.

2. Basic equations

For conical diffraction problems, we consider structures which are invariant in z and assume that the electromagnetic field depends on z as $e^{i\gamma_0 z}$ where γ_0 is a given nonzero constant. The dielectric function $\varepsilon(x, y)$ describing the structure is z independent and piecewise constant. In each homogeneous domain, every component of the electromagnetic field satisfies the

Helmholtz equation

$$\partial_x^2 u + \partial_y^2 u + (k_0^2 \varepsilon - \gamma_0^2) u = 0, \tag{1}$$

where k_0 is the free space wavenumber. The problem can be solved using two components of the electromagnetic field. The formulation given in [31] uses the two z components H_z and E_z. For non-magnetic media and gratings with corners, we use the x and y components of the magnetic field, since they are the smoothest functions among the six components [32]. Let Γ be an interface (discontinuity of ε), then H_x, H_y, H_z and E_z are continuous across Γ. The conditions for H_z and E_z imply that

$$\partial_x H_x + \partial_y H_y, \quad \frac{1}{\varepsilon}(\partial_y H_x - \partial_x H_y) \tag{2}$$

must be continuous.

We further assume that the structure is periodic in x with a period L, and the media in the top and bottom regions are homogeneous. If the top and bottom regions are given by $y > D$ for some positive D and $y < 0$, respectively, then the dielectric function satisfies $\varepsilon = \varepsilon^{(1)}$ for $y > D$ and $\varepsilon = \varepsilon^{(2)}$ for $y < 0$, where $\varepsilon^{(1)}$ and $\varepsilon^{(2)}$ are constants. In the top region, we specify a plane incident wave with a wave vector $(\alpha_0, -\beta_0^{(1)}, \gamma_0)$, then the reflected wave in the top region and the transmitted wave in the bottom region can be expanded in plane waves with wave vectors $(\alpha_j, \beta_j^{(1)}, \gamma_0)$ and $(\alpha_j, -\beta_j^{(2)}, \gamma_0)$, respectively, where j is an arbitrary integer and

$$\alpha_j = \alpha_0 + 2\pi j/L, \quad \beta_j^{(l)} = \sqrt{k_0^2 \varepsilon^{(l)} - \alpha_j^2 - \gamma_0^2}, \quad l = 1, 2. \tag{3}$$

Since the incident wave depends on x as $e^{i\alpha_0 x}$ and the structure is periodic in x, the electromagnetic field is quasi-periodic in x. That is

$$u(x + L, y) = e^{i\alpha_0 L} u(x, y), \tag{4}$$

where u is any field component. To simplify the notations, the dependence on z is removed.

The problem can be formulated on a rectangular domain $S = \{(x, y) \mid 0 < x < L, 0 < y < D\}$ based on the above quasi-periodic condition and two extra conditions at $y = 0$ and $y = D$. For the jth plane wave component of the transmitted wave, the partial derivative with respect to y is simply a multiplication by $-i\beta_j^{(2)}$. Therefore, if we define an operator $B^{(2)}$ such that $B^{(2)} e^{i\alpha_j x} = i\beta_j^{(2)} e^{i\alpha_j x}$ for all j, then the bottom boundary condition is

$$\partial_y u(x, 0^-) = -B^{(2)} u(x, 0). \tag{5}$$

We can also write down $B^{(2)}$ explicitly as

$$(B^{(2)} f)(x) = \frac{i}{L} \sum_{j=-\infty}^{\infty} \beta_j^{(2)} \int_0^L f(\tilde{x}) e^{i\alpha_j (x - \tilde{x})} d\tilde{x}, \tag{6}$$

where f is an any quasi-periodic function of x with period L and multiplier $e^{i\alpha_0 L}$. Similarly, the top boundary condition is

$$\partial_y u(x, D^+) = B^{(1)} u(x, D) - 2B^{(1)} u^{(i)}(x, D^+), \tag{7}$$

where $u^{(i)}$ is the given incident wave, $B^{(1)}$ is defined as $B^{(2)}$ with $\beta_j^{(2)}$ replaced by $\beta_j^{(1)}$. Notice that both H_x and H_y satisfy the same boundary conditions (5) and (7).

3. The BIE-NtD method

In this section, we present an improved BIE-NtD method for conical diffraction of gratings based on a modified NtD map and using the x and y components of the magnetic field. As in [30, 31], we first divide the rectangular domain S into a few subdomains Ω_j, for $j = 1$, ..., m. The dielectric function in Ω_j is a constant ε_j. The curves Γ_j $(1 \le j < m)$ separating these subdomains are located on the material interfaces. The top and bottom boundaries of S are the line segments Γ_m and Γ_0 at $y = D$ and $y = 0$, respectively. A typical example is shown in Fig. 1.

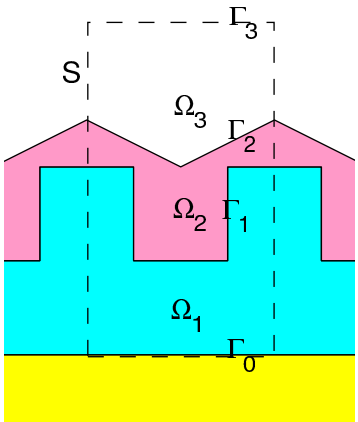

Fig. 1. A typical diffraction grating.

For any u satisfying Eq. (1) in a subdomain Ω_j, a BIE can be used to calculate the NtD operator that maps $\partial_\nu u$ (the normal derivative of u) to u on $\partial\Omega_j$ (the boundary of Ω_j) [30]. The integral equation can be discretized by a Nyström method with a graded mesh corresponding to a change of variable $s = w(t)$ (where s is the original parameter of $\partial\Omega_j$) and a uniform discretization in t [33]. The definition of w depends on a positive integer p. On a smooth piece of $\partial\Omega_j$ given by $s_b < s < s_e$, the new variable is given by $t_b < t < t_e$, and the function w is

$$w(t) = \frac{s_e w_1^p + s_b w_2^p}{w_1^p + w_2^p} \quad \text{for} \quad t_b \le t \le t_e, \tag{8}$$

where

$$w_1 = \left(\frac{1}{2} - \frac{1}{p}\right)\xi^3 + \frac{\xi}{p} + \frac{1}{2}, \quad w_2 = 1 - w_1, \quad \xi = \frac{2t - (t_b + t_e)}{t_e - t_b}.$$

Notice that on each smooth piece of $\partial\Omega_j$, $w(t)$ is a sigmoid function, and its derivatives up to the $(p-1)$th order vanish at the two end points. The graded mesh is used to resolve possible field singularities around corners, but it makes the NtD matrix nearly singular. In a recent work on optical waveguides [34], we found that numerically it is more stable to take out w' (the derivative of w) and calculate the modified NtD map $\mathcal{V}_j$ satisfying

$$\mathcal{V}_j\,\varphi = u \quad \text{on} \quad \partial\Omega_j, \tag{9}$$

where $\varphi = w'\partial_{\boldsymbol{\nu}} u$. The details for computing the original or modified NtD maps using BIEs are given in Refs. [30, 34]. Here, we assume that the unit normal vector $\boldsymbol{\nu}$ on Γ_j points into Ω_{j+1} (or $y > D$ if $j = m$), and $\boldsymbol{\nu}$ on Γ_{j-1} points into Ω_j. Since u satisfies the quasi-periodic condition (4), we can eliminate both u and φ on the vertical segments of $\partial\Omega_j$ [30]. This leads to the reduced NtD map $\mathcal{N}_j$ satisfying

$$\mathcal{N}_j \begin{bmatrix} \varphi_{j-1}^+ \\ \varphi_j^- \end{bmatrix} = \begin{bmatrix} \mathcal{N}_{j,11} & \mathcal{N}_{j,12} \\ \mathcal{N}_{j,21} & \mathcal{N}_{j,22} \end{bmatrix} \begin{bmatrix} \varphi_{j-1}^+ \\ \varphi_j^- \end{bmatrix} = \begin{bmatrix} u_{j-1} \\ u_j \end{bmatrix}, \tag{10}$$

where u_j denotes u on Γ_j, φ_j^+ and φ_j^- denote the one-sided limits of φ from above and below Γ_j, respectively. In the above, $\mathcal{N}_j$ is also given in 2×2 blocks.

To find the reflected and transmitted waves, we use an operator marching scheme that manipulates a pair of operators from the bottom ($y = 0^-$) to the top ($y = D^+$). For $\boldsymbol{u} = [H_x, H_y]^T$ and $\boldsymbol{\varphi} = w'\partial_{\boldsymbol{\nu}}\boldsymbol{u}$, we define the operators $\mathcal{Q}_j$ and $\mathcal{Y}_j$ satisfying

$$\mathcal{Q}_j^+ \boldsymbol{u}_j = \boldsymbol{\varphi}_j^+, \quad \mathcal{Q}_j^- \boldsymbol{u}_j = \boldsymbol{\varphi}_j^-, \quad \mathcal{Y}_j \boldsymbol{u}_j = \boldsymbol{u}_0, \tag{11}$$

where $\boldsymbol{u}_j$ denotes $\boldsymbol{u}$ on Γ_j, etc. Using these notations, the boundary conditions (5) and (7) can be written as

$$\boldsymbol{\varphi}_0^- = -\mathcal{B}^{(2)}\boldsymbol{u}_0 \quad \text{on} \quad \Gamma_0 \tag{12}$$

$$\boldsymbol{\varphi}_m^+ = \mathcal{B}^{(1)}\boldsymbol{u}_m + \boldsymbol{g}_m \quad \text{on} \quad \Gamma_m \tag{13}$$

where $\mathcal{B}^{(l)} = \text{diag}\{w'B^{(l)}, w'B^{(l)}\}$ for $l = 1, 2$, and $\boldsymbol{g}_m = -2\mathcal{B}^{(1)}\boldsymbol{u}^{(i)}|_{\Gamma_m}$. Clearly, $\mathcal{Y}_0$ is an identity operator. Eq. (12) gives $\mathcal{Q}_0^- = -\mathcal{B}^{(2)}$. Once $\mathcal{Q}_m^+$ and $\mathcal{Y}_m$ are obtained, we use Eq. (13), i.e., $(\mathcal{Q}_m^+ - \mathcal{B}_1)\boldsymbol{u}_m = \boldsymbol{g}_m$ to solve $\boldsymbol{u}_m$, and evaluate $\boldsymbol{u}_0$ by $\boldsymbol{u}_0 = \mathcal{Y}_m\boldsymbol{u}_m$.

To find $\mathcal{Q}_m^+$ and $\mathcal{Y}_m$, we need two types of marching steps: (1) propagation steps that calculate $\mathcal{Q}_j^-$ and $\mathcal{Y}_j$ from $\mathcal{Q}_{j-1}^+$ and $\mathcal{Y}_{j-1}$ for $1 \le j \le m$; (2) transition steps that calculate

$\mathcal{Q}_j^+$ from $\mathcal{Q}_j^-$ for $0 \le j \le m$. The jth propagation step can be derived from the reduced NtD map $\mathcal{N}_j$ satisfying Eq. (10). As in [31], we obtain

$$\mathcal{Z}_j = \left(\mathcal{I} - \begin{bmatrix} \mathcal{N}_{j,11} & \\ & \mathcal{N}_{j,11} \end{bmatrix} \mathcal{Q}_{j-1}^+\right)^{-1} \begin{bmatrix} \mathcal{N}_{j,12} & \\ & \mathcal{N}_{j,12} \end{bmatrix}, \tag{14}$$

$$\mathcal{Q}_j^- = \left(\begin{bmatrix} \mathcal{N}_{j,22} & \\ & \mathcal{N}_{j,22} \end{bmatrix} + \begin{bmatrix} \mathcal{N}_{j,21} & \\ & \mathcal{N}_{j,21} \end{bmatrix} \mathcal{Q}_{j-1}^+ \mathcal{Z}_j\right)^{-1}, \tag{15}$$

$$\mathcal{Y}_j = \mathcal{Y}_{j-1} \mathcal{Z}_j \mathcal{Q}_j^-. \tag{16}$$

A formula for the jth transition step can be derived from the condition that the two functions given in (2) must be continuous across Γ_j. Let $\boldsymbol{\nu} = (\nu_x, \nu_y)$ be the unit normal vector of Γ_j and $\boldsymbol{\tau} = (-\nu_y, \nu_x)$ be the unit tangential vector. Rewriting the partial derivatives of H_x and H_y as linear combinations of their normal and tangential derivatives and imposing the continuity conditions, we can find an equation connecting $\partial_{\boldsymbol{\nu}} \boldsymbol{u}_j^+$, $\partial_{\boldsymbol{\nu}} \boldsymbol{u}_j^-$ and $\partial_{\boldsymbol{\tau}} \boldsymbol{u}_j$. With a further multiplication of w' to both sides, we obtain

$$\boldsymbol{\varphi}_j^+ = \mathcal{M}_j \, \boldsymbol{\varphi}_j^- + \mathcal{T}_j \, \boldsymbol{\psi}_j, \tag{17}$$

where $\sigma_j = 1 - \varepsilon_{j+1}/\varepsilon_j$, $\boldsymbol{\psi}_j = w' \partial_{\boldsymbol{\tau}} \boldsymbol{u}_j$ and

$$\mathcal{M}_j = \begin{bmatrix} 1 - \sigma_j \nu_y^2 & \sigma_j \nu_x \nu_y \\ \sigma_j \nu_x \nu_y & 1 - \sigma_j \nu_x^2 \end{bmatrix}, \quad \mathcal{T}_j = \sigma_j \begin{bmatrix} -\nu_x \nu_y & -\nu_y^2 \\ \nu_x^2 & \nu_x \nu_y \end{bmatrix}. \tag{18}$$

This gives rise to the following transition formula

$$\mathcal{Q}_j^+ = \mathcal{M}_j \mathcal{Q}_j^- + \mathcal{T}_j \begin{bmatrix} w' \partial_{\boldsymbol{\tau}} & \\ & w' \partial_{\boldsymbol{\tau}} \end{bmatrix}. \tag{19}$$

4. Tangential derivative

In the previous version [31], a least squares method is used to approximate the tangential derivative operator $\partial_{\boldsymbol{\tau}}$ along the interfaces. This may have caused a reduced order of accuracy for the BIE-NtD method. In the current version, the transition formula (19) requires a matrix approximation for the scaled tangential derivative operator $w' \partial_{\boldsymbol{\tau}}$. We present an accurate method for approximating $w' \partial_{\boldsymbol{\tau}}$ based on the discrete Fourier transform.

Let the curve Γ_j be given by a parametric representation

$$\boldsymbol{r}(s) = (x(s), y(s)), \quad 0 \le s \le L_j. \tag{20}$$

A graded mesh on Γ_j is obtained by a change of variable $s = w(t)$ for $0 \le t \le T_j$ and a uniform discretization in t: $\{t_k = kT_j/N_j \ : \ 0 \le k < N_j\}$, where N_j is the total number of points

on Γ_j. For a scalar quasi-periodic function u given at the N_j mesh points: $u_k = u(\boldsymbol{r}(w(t_k))$, $0 \le k < N_j$, we need to approximate $\psi = w'\partial_{\boldsymbol{\tau}} u$ at these points. Since

$$\partial_{\boldsymbol{\tau}} u(\boldsymbol{r}) = \frac{1}{|\boldsymbol{r}'(s)|}\frac{du(\boldsymbol{r}(s))}{ds} = \frac{1}{w'(t)|\boldsymbol{r}'(w(t))|}\frac{du(\boldsymbol{r}(w(t)))}{dt},$$

where $|\boldsymbol{r}'(s)| = \sqrt{[x'(s)]^2 + [y'(s)]^2}$ and the prime denotes the derivative, we have

$$\psi(t) = \frac{1}{|\boldsymbol{r}'(\omega(t))|}\frac{du(\boldsymbol{r}(\omega(t)))}{dt}. \tag{21}$$

Since u is quasi-periodic in x, the function $h(t) = \exp[-i\alpha_0 x(w(t))]u(\boldsymbol{r}(w(t)))$ is a periodic function of t with period T_j, and

$$\frac{dh(t)}{dt} = e^{-i\alpha_0 x(w(t))}\left[-i\alpha_0\frac{dx(w(t))}{dt}u(\boldsymbol{r}(w(t))) + |\boldsymbol{r}'(w(t))|\psi(t)\right]. \tag{22}$$

Using h at the N_j points, i.e., $h_k = u_k \exp[-i\alpha_0 x(w(t_k))]$ for $0 \le k < N_j$, we first approximate $h(t)$ by

$$h(t) \approx \sum_{l=-N_j/2}^{N_j/2-1} \hat{h}_l \exp(i2\pi l t/T_j) \tag{23}$$

if N_j is even, where the coefficients are given by the discrete Fourier transform

$$\hat{h}_l = \frac{1}{N_j}\sum_{k=0}^{N_j-1} h_k e^{-i2\pi lk/N_j}, \quad -\frac{N_j}{2} \le l < \frac{N_j}{2}, \tag{24}$$

then evaluate the derivative of h at t_k by

$$\frac{dh}{dt}(t_k) \approx \sum_{l=-N_j/2}^{N_j/2-1} \frac{i2\pi l}{T_j}\hat{h}_l e^{i2\pi l t_k/T_j}, \quad k = 0, ..., N_j - 1. \tag{25}$$

Finally, we can evaluate ψ at t_k, $0 \le k < N_j$, by Eq. (22). The above steps give rise to a differentiation matrix $\mathcal{D}_j$, such that

$$\begin{bmatrix} \psi(t_0) \\ \psi(t_1) \\ \vdots \\ \psi(t_{N_j-1}) \end{bmatrix} \approx \mathcal{D}_j \begin{bmatrix} u_0 \\ u_1 \\ \vdots \\ u_{N_j-1} \end{bmatrix}. \tag{26}$$

The matrix $\mathcal{D}_j$ approximates $w'\partial_{\boldsymbol{\tau}}$ on Γ_j. The case for an odd N_j is similar.

5. Top and bottom boundary conditions

Since a graded mesh is used on the boundaries of all subdomains Ω_j, $1 \le j \le m$, the discretization points on the top and bottom line segments Γ_m and Γ_0 are not uniform. In the original BIE-NtD method [30], the boundary operators $B^{(1)}$ and $B^{(2)}$ are first approximated by matrices using a uniform discretization of x, then transformed to new matrices corresponding to the graded mesh points by a least squares method. This technique may also reduce the order of accuracy. Using the integral definition of the operators given in Eq. (6), we can approximate the boundary operators on the graded mesh points directly.

On the bottom boundary, the original parametric representation is $x = s$ and $y = 0$ for $0 \le s \le L$, and the graded mesh corresponds to the change of variable $x = w(t)$ for $0 \le t \le T_0$ and a uniform discretization $t_k = kT_0/N_0$ for $0 \le k < N_0$. We can approximate $B^{(2)}f$ in (6) by a truncation in j and a numerical integration by the trapezoidal rule in $\tilde{t}$, where $\tilde{x} = w(\tilde{t})$. That is

$$\begin{aligned}(B^{(2)}f)(x) &\approx \frac{i}{L}\sum_{j=-J_0}^{J_0}\beta_j^{(2)}e^{i\alpha_j x}\int_0^{T_0} f(w(\tilde{t}))e^{-i\alpha_j w(\tilde{t})}w'(\tilde{t})d\tilde{t} \\ &\approx \frac{iT_0}{LN_0}\sum_{j=-J_0}^{J_0}\beta_j^{(2)}e^{i\alpha_j x}\sum_{k=0}^{N_0-1} f(x_k)e^{-i\alpha_j x_k}w'(t_k),\end{aligned}$$

where $x_k = w(t_k)$. Applying the above approximation at $x_l = w(t_l)$ for $0 \le l < N_0$ and multiplying $w'(t_l)$, we obtain a linear relation between $f(x_k)$ for $0 \le k < N_0$, and $w'(t_l)(B^{(2)}f)(x_l)$ for $0 \le l < N_0$. The corresponding coefficient matrix is the approximation of $w'B^{(2)}$ on the graded mesh. The same approach applies to the operator $w'B^{(1)}$ at the top boundary.

After $\boldsymbol{u}$ at $y = D$ and $y = 0$ (i.e. $\boldsymbol{u}_m$ and $\boldsymbol{u}_0$) are obtained, we need to calculate the plane wave expansion coefficients of the transmitted and reflected waves. We use a numerical integration by the trapezoidal rule in the variable t. Consider a scalar u (which can be either H_x or H_y) in the bottom region where the transmitted wave is the total wave. If u is expanded as

$$u(x,y) = \sum_{j=-\infty}^{\infty} c_j \exp[i(\alpha_j x - \beta_j^{(2)} y)], \quad y \le 0, \tag{27}$$

then the coefficient c_j can be evaluated by

$$c_j = \frac{1}{L}\int_0^L u(x,0)e^{-i\alpha_j x}dx \approx \frac{T_0}{LN_0}\sum_{k=0}^{N_0-1} u(x_k,0)w'(t_k)e^{-i\alpha_j x_k}, \tag{28}$$

where $u(x_k, 0)$ for $0 \le k < N_0$, are given in $\boldsymbol{u}_0$. Similarly, the expansion coefficients of the reflected wave can be constructed from $\boldsymbol{u}_m$ after a subtraction by the incident wave.

6. In-plane diffraction problem

For in-plane diffraction problems of gratings, i.e. $\gamma_0 = 0$, the electromagnetic field can be decomposed to two separate polarizations. As usual, we use E_z for the transverse electric (TE) polarization and H_z for the transverse magnetic (TM) polarization, since these two components satisfy separate scalar Helmholtz equations. Notice that we cannot use H_x and H_y as in section 3, since H_x and H_y are both zero for the TM polarization. Furthermore, there is no need to evaluate tangential derivatives along material interfaces, since the interface conditions are very simple. Nevertheless, some ideas presented in the previous sections are still useful for the in-plane diffraction cases.

Unlike the original BIE-NtD method presented in [30], we use the modified NtD map $\mathcal{V}_j$ satisfying Eq. (9), where u is now either E_z or H_z. This leads to modified definitions of $\mathcal{Q}_j^{\pm}$ based on u_j and $\varphi_j^{\pm}$. For the TE and TM polarizations, $\partial_{\boldsymbol{\nu}} u$ and $\varepsilon^{-1}\partial_{\boldsymbol{\nu}} u$ are continuous across material interfaces, respectively. This leads the transition formula

$$\mathcal{Q}_j^{+} = \eta_j \mathcal{Q}_j^{-}, \tag{29}$$

where $\eta_j = 1$ for the TE polarization and $\eta_j = \varepsilon_{j+1}/\varepsilon_j$ for the TM polarization. The other steps are nearly identical to those given in sections 3 and 5. In particular, we use the new techniques to satisfy the top and bottom boundary conditions, and to calculate the expansion coefficients of the reflected and transmitted waves.

7. Numerical examples

In this section, we present a few numerical examples including both in-plane and conical diffraction cases. The first example was previously analyzed by the FMM and other numerical modal methods [14, 17]. It is the dielectric lamellar grating shown in Fig. 2(a). The period and the groove depth of the grating are $L = 2\,\mu$m and $d = 1\,\mu$m respectively. The dielectric constants of the top and bottom media are $\varepsilon^{(1)} = 1$ and $\varepsilon^{(2)} = 2.25$ respectively. The dielectric function of the grating layer satisfies $\varepsilon(x) = 5.29$ for $0 < x < 0.234L$ and $\varepsilon(x) = 1$ otherwise. We consider a plane incident wave with a free space wavelength $\lambda = 1\,\mu$m and a 30° incident angle with the y axis. We calculate the diffraction efficiency of the first transmitted order T_1 for the TM polarization. For this problem, we choose one period of the grating S and its three subdomain Ω_1, Ω_{21} and Ω_{22} as in Fig. 2(a), and let Ω_2 be the union of Ω_{21} and Ω_{22}. A simple modification is needed for the domain partition scheme given in section 3, since the high index subdomain Ω_{22} is surrounded by the low index subdomain Ω_{21} in the horizontal directions. After the modified NtD maps of Ω_{21} and Ω_{22} are calculated, we can eliminate the vertical and top boundaries of Ω_{22} and obtain the modified NtD map of Ω_2. More precisely, let the boundaries of Ω_{21} and Ω_{22} be $\Sigma_0 \cup \Sigma_1$ and $\Sigma_0 \cup \Sigma_2$, respectively, where Σ_0 is the common boundary of these two subdomains, i.e., the top and vertical sides of Ω_{22}.

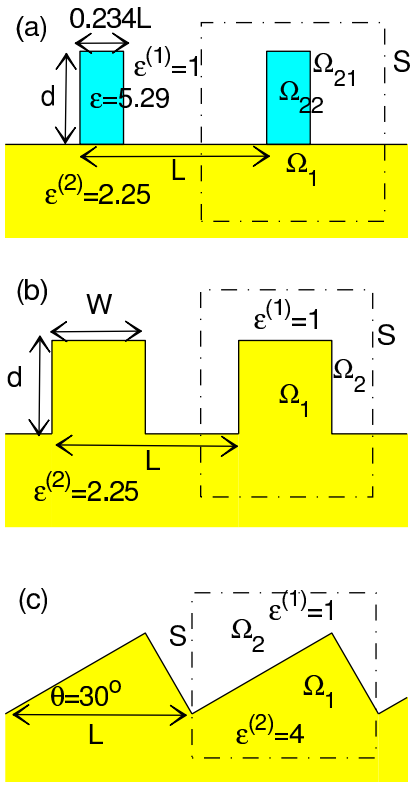

Fig. 2. Three dielectric diffraction gratings.

For in-plane diffraction problems, the modifed NtD maps of Ω_{21} and Ω_{22} provide relations between $u|_{\Sigma_0}$, $u|_{\Sigma_1}$, $u|_{\Sigma_2}$, $\varphi|^{\pm}_{\Sigma_0}$, $\varphi|_{\Sigma_1}$ and $\varphi|_{\Sigma_2}$, where $\varphi|_{\Sigma_1}$ and $\varphi|^{+}_{\Sigma_0}$ are one-sided limits of φ from Ω_{21}, and $\varphi|_{\Sigma_2}$ and $\varphi|^{-}_{\Sigma_0}$ are one-sided limits of φ from Ω_{22}. Using these relations and the interface condition on Σ_0, we can eliminate $u|_{\Sigma_0}$ and $\varphi|^{\pm}_{\Sigma_0}$, and obtain a relation between $u|_{\Sigma_1}$, $u|_{\Sigma_2}$, $\varphi|_{\Sigma_1}$ and $\varphi|_{\Sigma_2}$. This leads to the modified NtD map of Ω_2, since the boundary of Ω_2 is $\Sigma_1 \cup \Sigma_2$. For the conical diffraction case, the procedure is similar, but the interface condition (17) is vectorial, thus the modified NtD map of Ω_2 relate $\boldsymbol{\varphi}|_{\Sigma_1}$ and $\boldsymbol{\varphi}|_{\Sigma_2}$ with $\boldsymbol{u}|_{\Sigma_1}$ and $\boldsymbol{u}|_{\Sigma_2}$. The boundaries of Ω_{21}, Ω_{22} and Ω_1 consist of 8, 4 and 6 smooth segments, respectively. Using $p = 7$ and $N = 160$, where p is a parameter used in the graded mesh transform w and N is the number of points on each smooth segment of the boundaries, we obtain an accurate solution $T_1 = 0.5105923632003$. This result is consistent with previous calculations in [14,17]. If 499 terms are retained in the Fourier series, the standard FMM gives $T_1 = 0.510596$ [17]. Since the exact value of T_1 is not known, we compare the numerical solutions for different p and different N. Using the above value of T_1 as the reference solution, we calculate the absolute error for other approximate values of T_1 obtained using smaller values of p and N. The results are shown in Fig. 3 in a logarithmic scale, where the horizontal axis is $1/N$ and

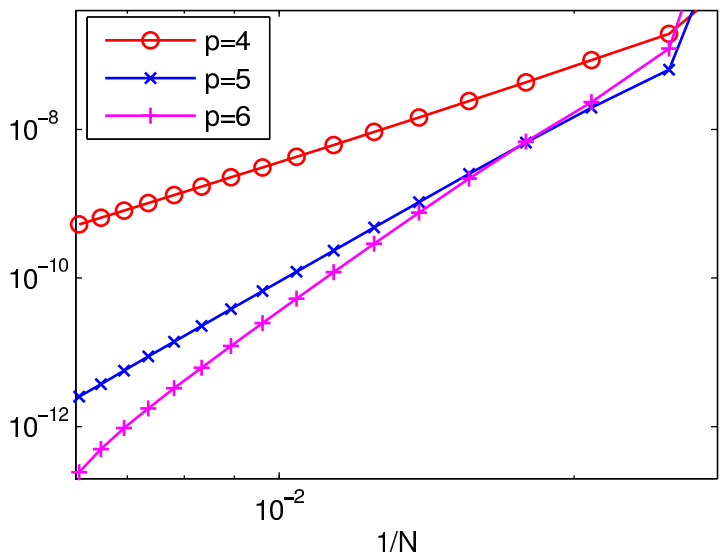

Fig. 3. Example 1: absolute error vs. $1/N$ for the diffraction efficiency of the first transmitted order.

the vertical axis is the absolute error. Apparently, as N is increased, the numerical solutions converge and the exact value of T_1 is very close to our reference solution above. For each fixed p, the slopes of the curves connecting the solutions for different N give the order of

accuracy of our method. It is clear that the order increases as p is increased. The exact value of the order is unknown. It appears that the order depends on the solution, especially, its behavior near the corners. A high order method is obtained, if we simply use a large p to define the graded mesh transform $s = w(t)$. However, if p is too large, the method becomes numerically unstable. Furthermore, for a fixed and relatively small N, the method may give less accurate solutions for larger p.

The second example is the dielectric lamellar grating shown in Fig. 2(b), where the period, the ridge width and the groove depth are $L = 1\,\mu$m, $W = 0.5\,\mu$m and $d = 0.5\,\mu$m, respectively, and the dielectric constants are $\varepsilon^{(1)} = 1$ and $\varepsilon^{(2)} = 2.25$ respectively. This problem was previously analyzed by an analytic modal method [10] and a BIE method [27]. We consider an incident wave with a free space wavelength $\lambda = 0.5\,\mu$m and a wave vector $(\alpha_0, -\beta_0^{(1)}, \gamma_0) = k_0(0.5, -\sqrt{0.5}, 0.5)$. The vector coefficient of the incident wave $\boldsymbol{u}^{(i)} = [H_x^{(i)}, H_y^{(i)}]^T$ is $(-\sqrt{0.5} + 0.5i, \sqrt{0.5}i)^T$. To use the BIE-NtD method, we consider one period of the grating S and its two subdomains Ω_1 and Ω_2 as in Fig. 2(b). Both $\partial\Omega_1$ and $\partial\Omega_2$ have 8 smooth segments. Using $p = 7$ and $N = 160$, we obtain a reference solution $T_1 = 0.37826780866$, where T_1 is the diffraction efficiency of the first transmitted order. This agrees with the previous results $T_1 = 0.37827$ given in [10] and $T_1 = 0.3783$ given in [27]. In Fig. 4. we show the absolute error vs. $1/N$ for other numerical solutions obtained with

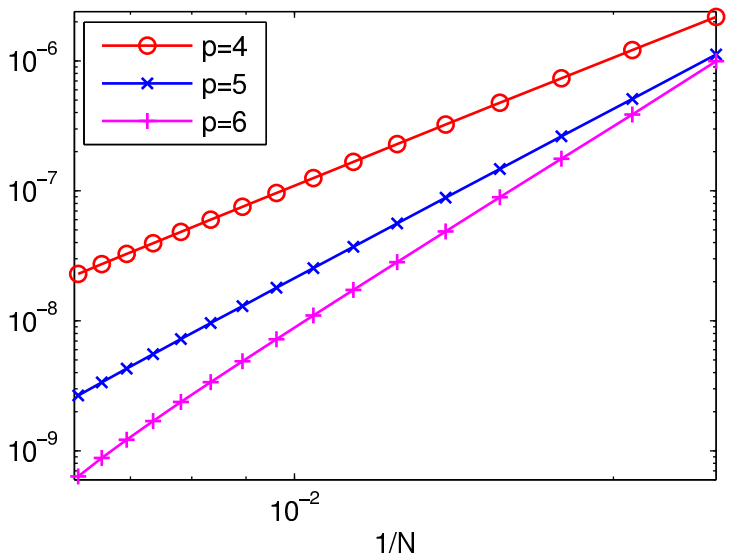

Fig. 4. Example 2: absolute error vs. $1/N$ for the diffraction efficiency of the first transmitted order.

smaller values of p and N. As before, the results are shown in a logarithmic scale and the

slopes of the curves indicate the order of the method.

The last example is a dielectric echelette grating as shown in Fig. 2(c). The dielectric constants of the top and bottom media are $\varepsilon^{(1)} = 1$ and $\varepsilon^{(2)} = 4$, respectively. The period and the blaze angle of the echelette grating are $L = 1\,\mu$m and $30°$, respectively. The incident wave has a free space wavelength $\lambda = 0.5\,\mu$m and a wave vector $(\alpha_0, -\beta_0^{(1)}, \gamma_0) = k_0(\sin 50° \cos 270°, \sin 50° \sin 270°, \cos 50°)$. The coefficient of the incident wave $\boldsymbol{u}^{(i)}$ is $(-\sin 270°, \cos 270°)^T$. To use the BIE-NtD method, we choose the domain S and its two subdomains Ω_1 and Ω_2 as shown in Fig. 2(c). The boundary of each subdomain has 5 smooth segments. Using $p = 8$ and $N = 184$, we obtain $T_1 = 0.55731295476$. The absolute errors of numerical solutions obtained with smaller values of p and N are shown in Fig. 5. The results again indicate high order of accuracy of our method for large p.

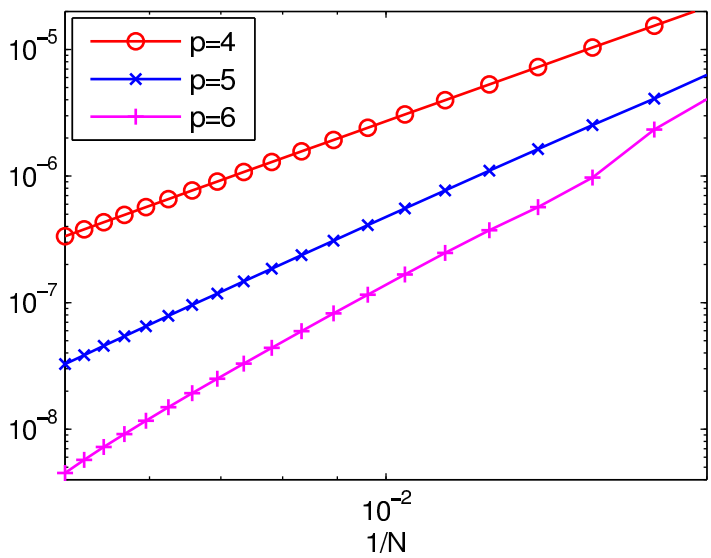

Fig. 5. Example 3: absolute error vs. $1/N$ for the diffraction efficiency of the first transmitted order.

8. Conclusion

In this paper, a high order BIE method for analyzing in-plane and conical diffraction problems of gratings is presented. The method is an improved version of the BIE-NtD method developed in earlier works [30,31]. The improvements include a modified NtD map for better numerical stability, a more accurate discretization for the boundary conditions connecting the top and bottom homogeneous regions, a new operator marching scheme using H_x and H_y, and an accurate method for computing tangential derivatives along material interfaces.

Note that the last two improvements are only applicable to conical diffractions. Numerical examples indicate that our improved BIE-NtD method achieves a high order of accuracy. The order depends on a parameter p used to specify the graded mesh and it may also depend on the solution and in particular the behavior of the electromagnetic field at the corners.

Acknowledgments

This research was partially supported by a grant from Hong Kong Research Grants Council (project number: CityU 102008).

References

1. R. Petit, ed., Electromagnetic Theory of Gratings (Springer-Verlag, Berlin, 1980).
2. G. Bao, L. Cowsar, and W. Masters, ed., Mathematical Modeling in Optical Sciences (Society for Industrial and Applied Mathematics, 2001).
3. G. Bao, Z. M. Chen, and H. J. Wu, "Adaptive finite-element method for diffraction gratings," J. Opt. Soc. Am. A **22**, 1106-1114 (2005).
4. L. C. Botten, M. S. Craig, R. C. McPhedran, J. L. Adams, and J. R. Andrewartha, "The dielectric lamellar diffraction grating," Optica Acta **28**, 413-428 (1981).
5. L. Li, "A modal analysis of lamellar diffraction gratings in conical mountings," J. Mod. Opt. **40**, 553-573 (1993).
6. M. Foresti, L. Menez, and A. V. Tishchenko, "Modal method in deep metal-dielectric gratings: the decisive role of hidden modes," J. Opt. Soc. Am. A **23**, 2501-2509 (2006).
7. S. Campbell, L. C. Botten, R. C. McPhedran, and C. M. de Sterke, "Modal method for classical diffraction by slanted lamellar gratings," J. Opt. Soc. Am. A **25**, 2415-2426 (2008).
8. P. Lalanne and G. M. Morris, "Highly improved convergence of the coupled-wave method for TM polarization," J. Opt. Soc. Am. A **13**, 779-784 (1996).
9. G. Granet and B. Guizal, "Efficient implementation of the coupled-wave method for metallic lamellar gratings in TM polarization," J. Opt. Soc. Am. A **13**, 1019-1023 (1996).
10. L. Li, "Use of Fourier series in the analysis of discontinuous periodic structures," J. Opt. Soc. Am. A **13**, 1870-1876 (1996).
11. N. M. Lyndin, O. Parriaux, and A. V. Tishchenko, "Modal analysis and suppression of the Fourier modal method instabilities in highly conductive gratings," J. Opt. Soc. Am. A **24**, 3781-3788 (2007).
12. I. Gushchin and A. V. Tishchenko, "Fourier modal method for relief gratings with oblique boundary conditions," J. Opt. Soc. Am. A **27**, 1575-1583 (2010).

13. R. H. Morf, "Exponentially convergent and numerically efficient solution of Maxwell's equations for lamellar gratings," J. Opt. Soc. Am. A **12**, 1043-1056 (1995).
14. P. Lalanne and J. P. Hugonin, "Numerical performance of finite-difference modal methods for the electromagnetic analysis of one-dimensional lamellar gratings," J. Opt. Soc. Am. A **17**, 1033-1042 (2000).
15. Y.-P. Chiou, W.-L. Yeh, and N.-Y. Shih, "Analysis of highly conducting lamellar gratings with multidomain pseudospectral method," J. Lightwave Technol. **27**, 5151-5159 (2009).
16. G. Granet, L. B. Andriamanampisoa, K. Raniriharinosy, A. M. Armeanu, and K. Edee, "Modal analysis of lamellar gratings using the moment method with subsectional basis and adaptive spatial resolution," J. Opt. Soc. Am. A **27**, 1303-1310 (2010).
17. D. Song, L. Yuan, and Y. Y. Lu, "Fourier-matching pseudospectral modal method for diffraction gratings", J. Opt. Soc. Am. A **28**, 613-620 (2011).
18. K. Edee, "Modal method based on subsectional Gegenbauer polynomial expansion for lamellar gratings," J. Opt. Soc. Am. A **28**, 2006-2013 (2011).
19. D. Maystre, Sur la Diffraction et l'Absorption par les Réseaux Utilisés dans l'Infrarouge, le Visible et l'Ultraviolet (PhD dissertation, Université d'Aix-Marseille III, France, 1974).
20. D. Maystre, "Integral Methods," in Electromagnetic Theory of Gratings, R.Petit, ed. (Springer-Verlag, Berlin, 1980), Chapter 3.
21. A. Pomp, "The integral method for coated gratings - computational cost," J. Mod. Opt. **38**, 109-120 (1991).
22. B. H. Kleemann, A. Mitreiter, and F. Wyrowski, "Integral equation method with parametrization of grating profile - Theory and experiments," J. Mod. Opt. **43**, 1323-1349 (1996).
23. D. W. Prather, M. S. Mirotznik, and J. N. Mait, "Boundary integral methods applied to the analysis of diffractive optical elements," J. Opt. Soc. Am. A **14**, 34-43 (1997).
24. E. Popov, B. Bozhkov, D. Maystre, and J. Hoose, "Integral method for echelles covered with lossless or absorbing thin dielectric layers," Appl. Opt. **38**, 47-55 (1999).
25. T. Magath and A. E. Serebryannikov, "Fast iterative, coupled-integral-equation technique for inhomogeneous profiled and periodic slabs," J. Opt. Soc. Am. A **22**, 2405-2418 (2005).
26. A. Rathsfeld, G. Schmidt, and B. H. Kleemann, "On a fast integral equation method for diffraction gratings," Commun. Comput. Phys. **1**, 984-1009 (2006).
27. L. I. Goray and G. Schmidt, "Solving conical diffraction with integral equations," J. Opt. Soc. Am. A **27**, 585-597 (2010).
28. G. Schmidt and B. H. Kleemann, "Integral equation methods from grating theory to photonics: an overview and new approaches for conical diffraction," J. Mod. Opt. **58**, 407-423 (2011).

29. E. Popov, M. Neviére, B. Gralak, and G. Tayeb, "Staircase approximation validity for arbitrary-shaped gratings," J. Opt. Soc. Am. A **19**, 33-42 (2002).
30. Y. Wu and Y. Y. Lu, "Analyzing diffraction gratings by a boundary integral equation Neumann-to-Dirichlet map method," J. Opt. Soc. Am. A **26**, 2444-2451 (2009).
31. Y. Wu and Y. Y. Lu, "Boundary integral equation Neumann-to-Dirichlet map method for gratings in conical diffraction," J. Opt. Soc. Am. A **28**, 1191-1196 (2011).
32. G. R. Hadley, "High-accuracy finite-difference equations for dielectric waveguide analysis II: Dielectric corners," J. Lightwave Technol. **20**, 1219-1231 (2002).
33. D. Colton and R. Kress, Inverse Acoustic and Electromagnetic Scattering Theory, 2nd ed., (Springer-Verlag, Berlin, 1998).
34. W. Lu and Y. Y. Lu, "Waveguide mode solver based on Neumann-to-Dirichlet operators and boundary integral equations," J. Comput. Phys. **231**, 1360-1371 (2012).